Applied Mathematics & Information Sciences
An International Journal

http://dx.doi.org/10.12785/amis/080101

LFAD: Locally- and Feature-Adaptive Diffusion based Image Denoising

Ajay K. Mandava[1,*], *Emma E. Regentova*[1] *and George Bebis*[2]

[1] Department of Electrical and Computer Engineering, University of Nevada, Las Vegas, NV 89154, USA
[2] Department of Computer Science and Engineering, University of Nevada, Reno, NV 89557, USA

Received: 18 May. 2013, Revised: 1 Sep. 2013, Accepted: 2 Sep. 2013
Published online: 1 Jan. 2014

Abstract: LFAD is a novel locally- and feature-adaptive diffusion based method for removing additive white Gaussian (AWG) noise in images. The method approaches each image region individually and uses a different number of diffusion iterations per region to attain the best objective quality according to the PSNR metric. Unlike block-transform based methods, which perform with a pre-determined block size, and clustering-based denoising methods, which use a fixed number of classes, our method searches for an optimum patch size through an iterative diffusion process. It is initialized with a small patch size and proceeds with aggregated (i.e., merged) patches until the best PSNR value is attained. Then the diffusion model is modified; instead of the gradient value, we use the inverse difference moment (IDM), which is a robust feature in determining the amount of local intensity variation in the presence of noise. Experiments with benchmark images and various noise levels show that the designed LFAD outperforms advanced diffusion-based denoising methods, and it is competitive with state-of-the-art block-transformed techniques; block and ring artifacts inherent to transform-based methods are reduced while PSNR levels are comparable.

Keywords: Diffusion, patch, region, over-segmentation

1 Introduction

Over the past decade, nonlinear anisotropic diffusion has drawn considerable attention and experienced significant developments, as it effectively diffuses noise in the intra-regions while inhibiting inter-region smoothing. First introduced by Perona and Malik (PM diffusion) [1], the diffusion process is mathematically described by the following equation:

$$\frac{\partial}{\partial t}I(x,y,t) = \nabla \bullet (c(x,y,t)\nabla I) \tag{1}$$

where I(x,y,t) is an image, t is the iteration step and c(x,y,t) is the monotonically decreasing function of the image gradient called diffusion function. Two diffusivity functions that have been proposed are:

$$c_1(x,y,t) = \exp\left(-\left(\frac{|\nabla I(x,y,t)|}{\lambda}\right)^2\right) \tag{2}$$

and

$$c_2(x,y,t) = \frac{1}{1+\left(\frac{|\nabla I(x,y,t)|}{\lambda}\right)^2} \tag{3}$$

where λ is referred to as the diffusion constant. Depending on the choice of the diffusivity function, Equation (1) covers a variety of filters. The discrete diffusion structure is translated into the following form:

$$I_{i,j}^{n+1} = I_{i,j}^{n} + (\nabla t) \bullet \begin{bmatrix} c_N\left(\nabla_N I_{i,j}^n\right)\bullet\nabla_N I_{i,j}^n + c_S\left(\nabla_S I_{i,j}^n\right)\bullet\nabla_S I_{i,j}^n + \\ c_E\left(\nabla_E I_{i,j}^n\right)\bullet\nabla_E I_{i,j}^n + c_W\left(\nabla_W I_{i,j}^n\right)\bullet\nabla_W I_{i,j}^n \end{bmatrix} \tag{4}$$

Subscripts N, S, E, and W (North, South, East, and West) describe the direction of the local gradient, and the local gradient is calculated using nearest-neighbor differences as

$$\begin{aligned} \nabla_N I_{i,j} &= I_{i-1,j} - I_{i,j}; \nabla_S I_{i,j} = I_{i+1,j} - I_{i,j} \\ \nabla_E I_{i,j} &= I_{i,j+1} - I_{i,j}; \nabla_W I_{i,j} = I_{i,j-1} - I_{i,j} \end{aligned} \tag{5}$$

The model in [1] has several practical and theoretical limits. It needs a reliable estimate of image gradients

* Corresponding author e-mail: mandavaa@unlv.nevada.edu

because with an increase in noise level, the effectiveness of the gradient calculation degrades and thus deteriorates the performance of the method. Furthermore, an equal number of iterations in the diffusion of all pixels in the image lead to blurring of textures and fine edges while the smooth regions benefit. For demonstration, let us apply PM diffusion to two different image patches, each representing a certain structural content, e.g., a texture and a smooth region. Fig. 1 indicates significant differences in PSNR values versus iteration numbers for the provided examples. The examples in Fig. 2 show how image quality varies between images denoised using two different iteration numbers, i.e., 22 and 30. In the left image, pixels are corrupted in a smooth region, and in the right, details are severely blurred.

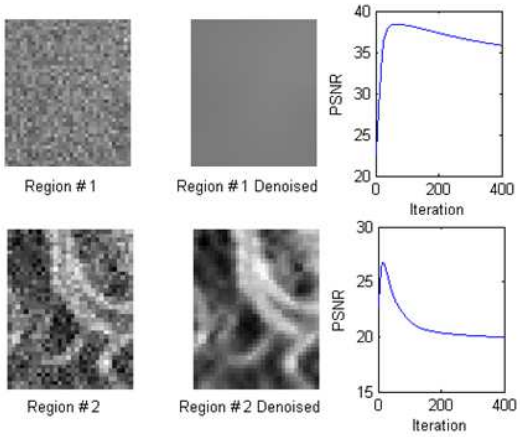

Fig. 1: Denoising results for two different structural contents.

Generally, the effectiveness of the anisotropic diffusion is determined by (a) the efficiency of the edge detection operator to distinguish between noise and edges; (b) the accuracy of an "edge-stopping" function to promote or inhibit diffusion; and (c) the adaptability of a convergence condition to terminate the diffusion process automatically. Research on diffusion-based denoising targets one or more of the above factors. Catte et al. [2] used a smoothed gradient of the image, rather than the true gradient. Let G_σ be a smoothing kernel; then

$$\frac{\partial}{\partial t}I(x,y,t) = \nabla \bullet (c(\|\nabla G_\sigma * I\|)\nabla I) \qquad (6)$$

The smoothing operator removes some of the noise that might have deceived the original PM filter. In this case, the scale parameter σ is fixed. In [3], the authors have proposed inhomogeneous anisotropic diffusion that includes separate multiscale edge detection. Yu et al. [4] have incorporated the SUSAN edge detector into the model:

$$\frac{\partial}{\partial t}I(x,y,t) = \nabla \bullet (SUSAN(c(\|\nabla G_\sigma * I\|))\nabla I) \qquad (7)$$

Due to noise suppression, the SUSAN can guide the diffusion process in an effective manner. Li et al. [5] proposed a context-adaptive anisotropic diffusion via a weighted diffusivity function. It is represented by the equation

$$\frac{\partial}{\partial t}I(x,y,t) = \nabla \bullet (w(x,y,t)c(x,y,t)\nabla I) \qquad (8)$$

where the combined term *w(x,y,t)c(x,y,t)* is referred to as the weighted diffusivity function and *w(x,y,t)* is a pixel-wise feature dependent weight function.

Fig. 2: PM denoised "Lena" image for two different iteration numbers (left = 22 iterations, PSNR = 29.37 dB; right = 30 iterations, PSNR = 28.52 dB) for AWG noise level, σ =20.

Chao and Tsai [6] proposed a diffusion model which incorporates both the local gradient and gray-level variance. High levels of noise produce larger magnitudes of variance and gradients than those by objects and textures. Thus, the method becomes inefficient for high noise levels. Wang et al. [7] studied a local variance controlled scheme wherein the spatial gradient and contextual discontinuity of a pixel are jointly employed to control the evolution. However, a solution to estimating the contextual discontinuity requires an exhaustive search procedure, which causes the algorithm to be too computationally expensive. Yu and Acton [8] proposed speckle-reducing anisotropic diffusion (SRAD), which integrated spatially adaptive filters into the diffusion and provided considerable improvement in speckle suppression over other conventional diffusion methods. Abd-Elmoniem et al. [9] devised a coherence-enhancing nonlinear coherent diffusion (CENCD) model for speckle reduction. This method combines isotropic diffusion, anisotropic coherent diffusion, and mean curvature motion. The aim is to maximally filter those regions which correspond to fully developed speckle while

preserving information associated with object structures. Zhang et al. [10] presented a Laplacian pyramid-based nonlinear diffusion (LPND) method where a Laplacian pyramid was utilized as a multiscale analysis tool to decompose an image into sub-bands. Then, anisotropic diffusion of a variable flux is applied to different subbands was used to suppress noise in each sub-band. LPND tries to introduce sparsity and multiresolution properties of multiscale analysis into anisotropic diffusion. Another approach to context-based diffusion was researched in [11]. Multi-scale stationary wavelet analysis of the local neighborhood across the scales provides edge information partially free of noise and thus makes tunable diffusion possible. As a result, due to the shift invariance property of the stationary wavelet transform, the PSNR has been improved, compared to Shih's diffusion [12].

State-of-the art denoising techniques all rely on patches, whether for dictionary learning [13,14], collaborative denoising of blocks of similar patches [15], or non-local sparse models [16]. Regularization with non-local patch-based weights has shown improvements over classical regularization involving only local neighborhoods [17,18,19]. The shape and size of patches should adapt to anisotropic behavior of natural images [20,21]. In spite of the high performance of patch-based denoising methods, they generally produce artifacts even at comparatively moderate noise levels.

Fig. 3: Results of two patch-based denoising methods: a) KLLD[14] denoising for σ = 25 and b) BM3D[15] denoising for σ = 60.

Examples of such visual artifacts are presented in Fig. 3 for two state-of-the-art methods, i.e., KLLD [14] and BM3D [15]. The size of the patch has a significant impact on the PSNR value even for similar or identical contents. Fig .4 shows that equal-size regions of the same structural content from different parts of the image could be diffused differently. Thus, both the structural content and the location of the patch are to be taken into account. Unlike block-transform based methods such as BM3D, which perform with a pre-determined optimum block size, and clustering-based denoising methods, such as KLLD, which use a predetermined optimum number of classes, our method searches for an optimum patch size through iterative diffusion starting with a small patch size, and proceeds with aggregating patches until a best PSNR is attained. We use superpixel segmentation [22] because it produces an over-segmented image of almost equally-sized patches, and thus is the best choice for initializing the method. We explain the selection of the initial number of patches, or, alternatively, the initial size of the patch for different noise levels. To determine the amount of diffusion, we use the inverse difference moment (IDM) feature [23]. We demonstrate that the feature is robust in estimating local intensity variation in the presence of noise. Overall, the diffusion process converges to PSNR levels comparable to those reported by state-of-the-art methods with less visible blocking/patching artifacts. The method is called locally- and feature-adaptive diffusion (LFAD). In Section 2 we introduce the method and provide implementation details. Section 3 presents experimental results; thereafter we conclude in the last section.

2 LFAD: Locally- and Feature-Adaptive Diffusion

The method performs as follows: a) image is over-segmented to k approximately equally-sized patches; b) each patch (region) is diffused individually until a best PSNR is attained; c) adjacent regions are merged based on a similarity metric; d) diffusion repeats for merged regions until PSNR shows improvement or only two regions are left covering the whole image. Subsections below discuss each of the above steps.

2.1 Superpixel Segmentation

As discussed above, we need to start with an over-segmented image. For this purpose, we use the superpixel segmentation method with a parameter k which is a desired number of approximately equally-sized superpixels. The procedure begins with an initialization step in which k initial cluster centers C_i are sampled on a regular S- pixel grid space. To produce roughly equally sized superpixels, the grid interval, S is set: $S = \sqrt{N/k}$. The centers are moved to seed locations corresponding to the lowest gradient position in a 3x3 neighborhood, and thus avoid centering a superpixel on an edge. This reduces the chance of seeding a superpixel with a noisy pixel. Next, in the assignment step, each pixel i is associated with the nearest cluster center whose search region overlaps its location. The distance measure D, determines the nearest cluster center for each pixel. Since the expected spatial extent of a superpixel is a region of approximate size SxS, the search for similar pixels is carried in a region of size 2Sx2S around the superpixel

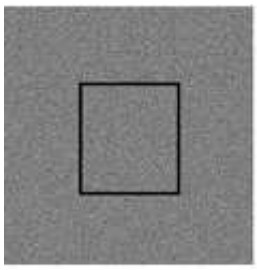

(a) Noisy Image σ = 20

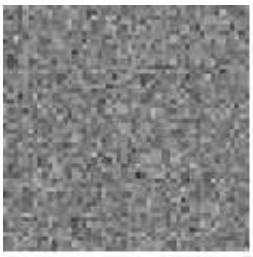

(b) Inside the square

(c) Diffusion outcome (PSNR = 73.54 dB)

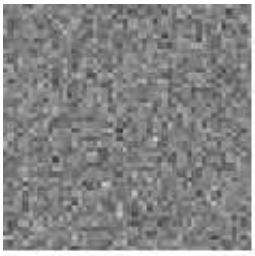

(d) Outside the square

(e) Diffusion outcome (PSNR = 65.71 dB)

Fig. 4: Diffusion results of structurally identical patches.

center. Once each pixel has been associated with the nearest cluster center, an update step adjusts the cluster centers to be the mean vector of all the pixels belonging to the cluster. The L2 norm is used to compute a residual error E between center locations of the new and previous clusters. The assignment and update steps can be repeated iteratively until convergence. Experimentally, twenty iterations are sufficient for most images, therefore, in the rest of the paper we use this value.

2.2 Region (patch) Merging

If image I is partitioned into sub-regions $R_1, R_2, \ldots, R_{n.}$ the following properties must hold true:

1.$R_1 \cup R_2 \cup \ldots \cup R_n = I$;
2. R_i *is connected;*
3. $R_i \cap R_j$ *is empty.*

The regions are merged based on the similarity metric which is chosen to be the intensity variance. Let us denote a pair of adjacent regions $R_i \tilde{} R_j$ and merged regions $R_i \cup R_j$. The region merging algorithm performs according to the following steps:

1.For $\forall\, R_i \tilde{} R_j$, if $\sigma_j{}^2 = \alpha * \sigma_i{}^2$ then $R_m = R_i \cup R_j$
2. If $R_m \neq I$, Increment α. Goto Step 1; otherwise
3. Stop.

2.3 Modified Diffusion

The normalized inverse difference moment (IDM) characterizes both coarse and fine structures. The IDM has small contributions from homogenous region and larger values from non-homogenous regions. Ranging between 0 and 1, a value of IDM equal to 0 indicates a pixel being part of a homogenous neighborhood. A value equal to 1 indicates that the pixel is a part of texture or an object boundary. The visualized IDM feature is contrasted with the gradient image in Fig. 5. IDM is calculated in 9x9 windows centered at pixel (i,j). Fig. 6 shows the line profile plots for both IDM and gradient values across the hat area of the "Lena" image with AWG noise σ=40. The figures show that IDM is a robust indicator of the object boundary and texture edges. The diffusivity function of Eq. 2 and 3 is modified to the following:

$$c_p = \exp\left(-\left(\frac{IDM(I)}{\lambda}\right)^2\right), p = N,S,W,E$$
$$\textit{and} \qquad (9)$$
$$c_p = \frac{1}{1+\left(\frac{IDM(I)}{\lambda}\right)^2}, p = N,S,W,E$$

where

$$IDM = 1 - \sum_{i=0}^{G-1}\sum_{j=0}^{G-1}\frac{1}{1+(i-j)^2}P(i,j) \qquad (10)$$

Given an MxN neighborhood containing G gray levels, let *f(m,n)* be the intensity at sample m, line n of the neighborhood. Then

$$P(i,j|\Delta x,\Delta y) = W \cdot Q(i,j|\Delta x,\Delta y)$$

where

$$W = \frac{1}{(M-\Delta x)(N-\Delta y)};$$
$$Q(i,j|\Delta x,\Delta y) = \sum_{n=1}^{N-\Delta y}\sum_{m=1}^{M-\Delta x} A$$

and

$$A = \left\{ \begin{array}{ll} 1, & if\, f(m,n) = i \;\; and \;\; f(m+\Delta x, n+\Delta y) = j \\ 0, & elsewhere \end{array} \right\}$$

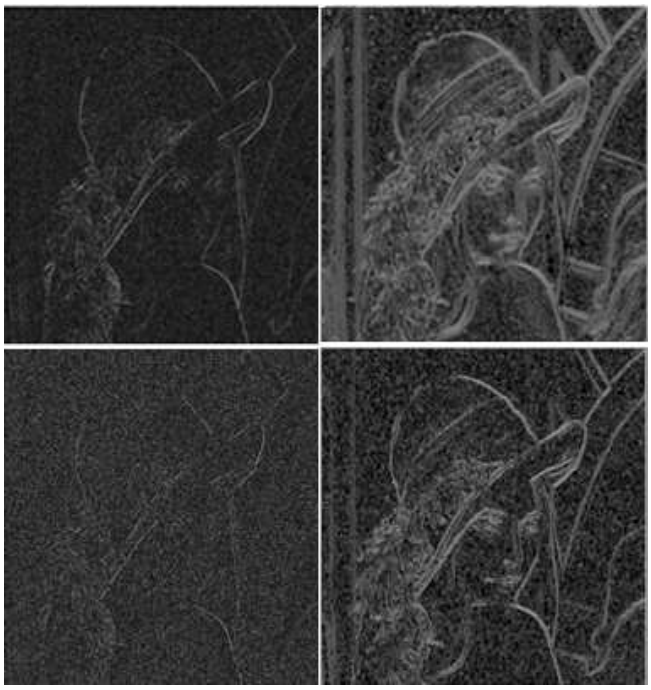

Fig. 5: First column: Gradient image for AWG noise σ =20, 40 for ”Lena”; Second column: IDM image for AWG noise σ=20, 40.

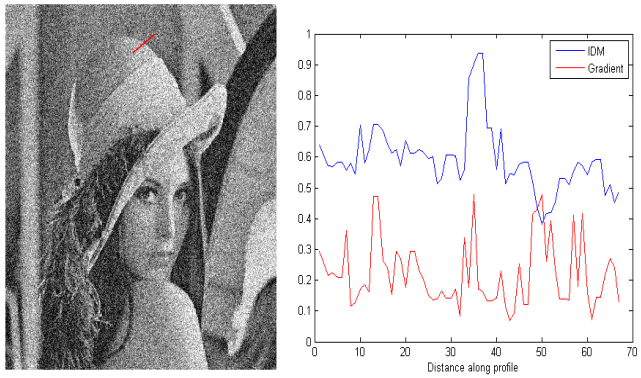

Fig. 6: Left: ”Lena” image with AWG noise σ =40; Right: IDM and gradient values along a line (red) segment in the ”Lena” image.

2.4 Parameter Selection: Patch Size and Diffusion Constant

Levin and Nadler [24] derive bounds on how well any denoising algorithm can perform. The bounds are dependent on the patch size, where larger patches lead to better results. For large patches and low noise, tight bounds cannot be estimated. The result suggests a novel adaptive variable-sized patch scheme for denoising. Chatterjee [25] found that smaller patches can lead to performance degradation from the lack of information captured by each patch, and large patches might capture regions of widely varying information in a single patch and also result in fewer similar patches being present in the image. It was shown also that clusters with more patches are denoised better than clusters with fewer patches, and the bound on the predicted MSE increases at different rates as the patch size grows from 5x5 to 19x19. Thus, it was concluded that a patch size of 11x11 can capture the underlying patch geometry while offering sufficient robustness in the search for similar patches. The BM3D uses blocks of 8x8 for low noise levels, i.e.,σ<=40 and 11x11 for the Wiener filter at the post processing step, and 12x12 patches for hard thresholding of transform coefficients for noise levels with σ>40.

Fig.7 displays the relationship between PSNR versus patch area size for noise levels σ=20 and σ=50 for the ”Lena” image. It clearly shows that for the low noise level σ=20, PSNR reaches its maximum around a patch area size of 50-80, and for the high noise level σ=50, PSNR reaches its maximum around a patch area size of 110-140. In our work, we calculate the bounds with a patch area of 64 pixels for low noise levels, i.e.,σ<=40, and a larger patch of 120 pixels for high noise levels, i.e.,σ>40. To make an automatic selection of the patch size, one can use one of several available methods for estimation of the noise standard deviation. For example, one can suppress the image structure using the Laplacian mask such that the remaining part of the image is noise [26].

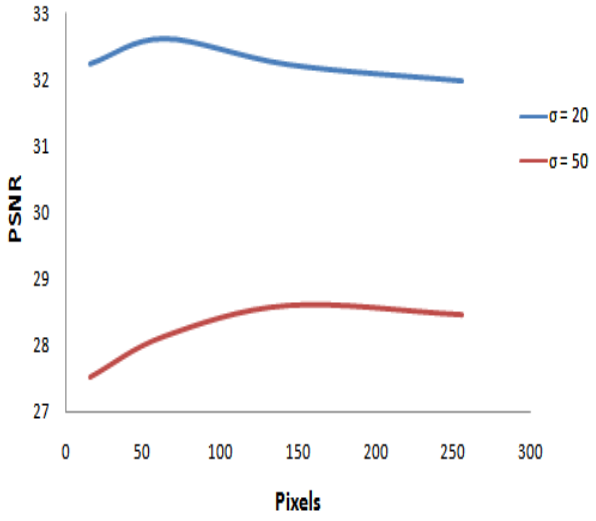

Fig. 7: PSNR versus patch size (area in pixels) with AWG noise σ=20 and σ=50 for the ”Lena” image.

The diffusion equation needs the value of the diffusion constant, λ. Fig. 8 displays PSNR values of the outcomes of IDM based diffusion for a fixed noise level (σ=50) with different values of λ (i.e., λ = 5, 10, 15, 25, and 50) for

1000 iterations for the ”Lena” image. The plot indicates that λ=10 is the best choice.

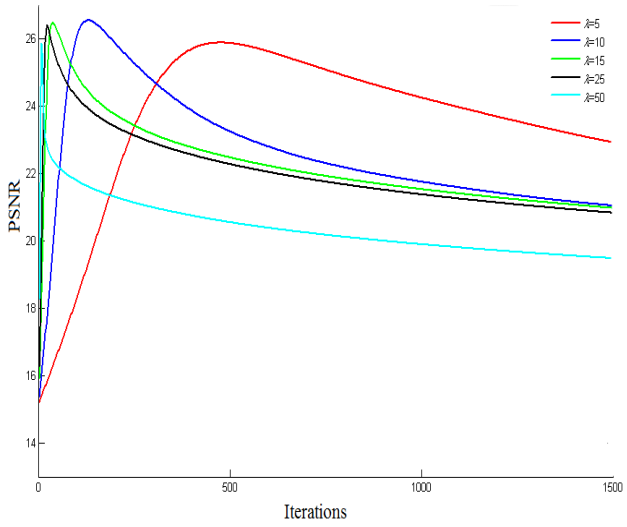

Fig. 8: PSNR obtained using IDM with λ=5, 10, 15, 25, and 50 with AWG noise σ=50 for the ”Lena” image.

2.5 LFAD Algorithm

Let us denote I - input image, k - number of regions, m - number of merging steps, Var -intensity variance and n - number of diffusion steps. The method performs according to the following steps:

1. *Initialize m=0, α = 1.1, λ =10. Segment image into k ($k \neq 1$) regions.*
2. *Initialize n=0. Calculate PSNR for each region of initial partition, i.e.,$[PSNR_k{}^{(0)}]_0$.*
3. *Iteration step: Diffuse image pixel $I_{i,j}$using Eq.(4).*
4. *For $\forall R_i$: if $[PSNR_k{}^{(n+1)}]_m > [\ PSNR_k{}^{(n)}]_m$, Goto Step 3; else Goto Step 6.*
5. *While $R_m \neq I$, for $\forall$ Ri ˜ Rj, if $Var(R_j) = \alpha * Var(R_i)$, then $R_i \cup R_j$; m=m+1; update k;, Goto Step 2, else Repeat Step 5 with $\alpha = \alpha + 0.1$.*
6. *Stop.*

3 Experimental Results

The LFAD is tested on a number of benchmark images degraded by AWG noise of μ=0 and σ = 10, 20, 30, 50, and 100. The comparison is made to other diffusion models such as PM[1], Catte[2], Li[5], LVCFAB[7], GSZFAB[27], and RAAD[28]. We also compare the method to the state-of-the-art denoising BM3D method. The evaluation is performed first based on PSNR calculated as follows:

$$PSNR = 10 \log \frac{I_{\max}^2}{MSE} \tag{11}$$

where MSE is a mean square error. Additionally, we evaluate the method using the universal image quality index (UIQI) given by

$$Q = \frac{4\sigma_{xy}\bar{x}\bar{y}}{\left(\sigma_x^2 + \sigma_y^2\right)\left[(\bar{x})^2 + (\bar{y})^2\right]} \tag{12}$$

where $\bar{x}$, $\bar{y}$ are the means; σ_x , σ_y are the standard deviations; σ_{xy} is the covariance. As mentioned in [29], the average quality index UIQI reflects the mean subjective ranks of observers.

The above specified parameters were used to obtain Table 1, which shows PSNR values by the LFAD for benchmark images. Next, in Table 2, the LFAD is compared to the six diffusion based methods. The improvement by LFAD for the given noise levels ranges from 1.3 dB for low noise to 1.59dB for AWG noise σ=100. It is interesting to note that, compared to the reference PM method, the use of the IDM feature helped with improving PSNR by 0.65db for low noise levels to 1.03 dB for higher noise.

The comparison to the state-of-the-art denoising method, i.e., BM3D, shows that the performance of LFAD is 0.35 dB lower compared to that of the BM3D for noise level σ=10 and 0.39 dB lower for noise level σ=100. Results for BM3D are publicly available at http://www.cs.tut.fi/˜foi/GCF-BM3D/index.html and therefore are not reproduced here. Table 3 provides UIQI values by the LFAD and BM3D, and Table 4 provides UIQI values by the LFAD and state-of-the-art diffusion models for same benchmark images. It follows from Tables 3 and 4 that according to this metric the proposed method outperforms the state-of-the-art diffusion models. Only for the ”Cameraman” image with AWG noise, σ=10 it shows lower performance. The proposed method shows similar as to BM3D. For high noise, i.e. σ=10 in ”Peppers” image, the proposed method outperforms BM3D. Fig. 9 shows that fewer blocking/ringing artifacts are introduced by LFAD than by the BM3D. The denoising performance of the LFAD is further illustrated in Fig. 10 and Fig. 11, where we show fragments of noisy (i.e., σ=10, 20, 30, and 50) test images and corresponding denoised fragments. It is notable that in the regions of smooth intensity transition, the quality of denoising is higher, and lesser or no ringing is observed around contours of extended objects.

Table 1: PSNR of the proposed method LFAD.

Image/Noise, σ	10	20	30	50	100
Lena	35.56	32.61	30.85	28.59	25.56
House	35.94	32.93	31.11	28.68	25.12
Peppers	34.48	31.05	29.03	26.56	23.18
Cameraman	33.99	30.18	28.24	25.89	23.08

Table 2: PSNR comparison of different anisotropic diffusion methods for "Lena".

Method/ σ	10	15	20
Noisy	28.15	24.62	22.14
PM [1]	32.70	30.71	29.37
Catte [2]	33.27	31.39	30.09
Li [5]	34.28	32.41	31.15
GSZ FAB [27]	32.49	29.86	28.29
LVCFAB [7]	31.90	28.21	26.67
RAAD [28]	34.33	32.53	31.24
LFAD	**35.56**	**33.86**	**32.61**

Table 3: UIQI comparison of BM3D and LAFD methods.

	10		20		30		50		100	
	BM3D	LFAD	BM3D	LFAD	BM3D	LFAD	BM3D	LFAD	BM3D	LFAD
Lena	0.6976	0.6903	0.6107	0.5991	0.5489	0.5391	0.4661	0.4566	0.3440	0.3427
House	0.5894	0.5640	0.4505	0.4296	0.4001	0.3810	0.3443	0.3224	0.2691	0.2411
Peppers	0.8182	0.8148	0.7443	0.7361	0.6863	0.6777	0.6016	0.5931	0.4664	**0.4682**
Cameraman	0.5975	0.5908	0.4914	0.4908	0.4319	0.4275	0.3567	0.3496	0.2600	0.2383

Table 4: UIQI comparison of anisotropic diffusion methods.

Scheme	Image	10	15	20
GSZ FAB	Lena	0.6294	0.5391	0.4833
	Peppers	0.592	0.5237	0.4682
	Cameraman	0.539	0.4333	0.3789
LVCFAB	Lena	0.6309	0.4955	0.4337
	Peppers	0.5883	0.4819	0.4236
	Cameraman	0.5441	0.3967	0.3413
RAAD	Lena	0.6819	0.6232	0.5749
	Peppers	0.6325	0.5764	0.5395
	Cameraman	**0.5994**	0.5199	0.4622
LFAD	Lena	**0.6903**	**0.6396**	**0.5991**
	Peppers	**0.8148**	**0.7708**	**0.7361**
	Cameraman	0.5908	**0.5314**	**0.4908**

Fig. 9: First row: ”Lena” image and that with AWG noise, σ =100; Second row: Results by BM3D and LFAD. Arrows show areas where LFAD performs comparatively better than BM3D.

Fig. 10: First column: ”Lena” image with AWG noise, σ =10, 20, 30, and 50; Second column: corresponding results by the LFAD.

Fig. 11: First column: ”Peppers” image with AWG noise, σ =10, 20, 30, and 50; Second column: corresponding results by LFAD.

4 Conclusion

We have proposed a new locally- and feature-adaptive diffusion based method of image denoising from AWG noise. The high performance of the method stems from the following properties: a) patch-based optimization of PSNR; b) region merging and repetitive iteration of the process; and c) modification of the diffusion function, i.e. usage of the IDM feature instead of the gradient value. The method has attained the highest performance in the class of advanced diffusion based methods. It is also competitive with the state-of-the-art BM3D method. Visible blocking and ringing artifacts generally inherent to block- and transform-based methods are reduced.

Acknowledgement

This research is supported by NASA EPSCoR under Cooperative Agreement No. NNX10AR89A.

References

[1] P. Perona and J. Malik, ”Scale-space and edge detection using anisotropic diffusion”, IEEE Transactions on Pattern Analysis and Machine Intelligence, **12**, 629-639 (1990).
[2] F. Catt, P.-L. Lions, J.-M. Morel, and T. Coll, ”Image selective smoothing and edge detection by nonlinear diffusion”, SIAM Journal on Numerical Analysis, **29**, 182-193 (1992).
[3] V. B. S. Prasath and A. Singh, ”Well-Posed Inhomogeneous Nonlinear Diffusion Scheme for Digital Image Denoising”, Journal of Applied Mathematics, **2010**, 14 pages (2010).
[4] J.Yu, J. Tan, Y. Wang, ”Ultrasound speckle reduction by a SUSAN-controlled anisotropic diffusion method”, Pattern Recognition, **2010**, 3083-3092.
[5] H. C. Li, P. Z. Fan, and M. K. Khan, ”Context-Adaptive Anisotropic Diffusion for Image Denoising”, IET Electronics Letters, **48**, 827-829 (2012).
[6] Shin-Min Chao, Du-Ming Tsai, ”An improved anisotropic diffusion model for detail- and edge-preserving smoothing”, Pattern Recognition Letters, **31**, 2012-2023 (2010).
[7] Y. Wang, L. Zhang, P. Li, ”Local Variance-Controlled Forward-and-Backward Diffusion for Image Enhancement and Noise Reduction”, IEEE Transactions on Image Processing, 1854-1864 (2007).
[8] Y. Yu and S.T. Acton, ”Speckle reducing anisotropic diffusion”, IEEE Transactions on Image Processing, **11**, 1260-1270 (2002).
[9] Z. Fan, Mo Yoo Yang, Mong Koh Liang, and Kim Yongmin, ”Nonlinear Diffusion in Laplacian Pyramid Domain for Ultrasonic Speckle Reduction”, IEEE Transactions on. Medical Imaging, **26**, 200-211 (2007).
[10] K. Z. Adb-Elmoniem , A. M., Youssef , and Y. M. Kadah, ”Real-time speckle reduction and coherence enhancement in ultrasound imaging via nonlinear anisotropic diffusion” , IEEE Transactions on Biomedical Engineering, **49**, 997-1014 (2002).
[11] A. K. Mandava and E.E. Regentova, ”Image denoising based on adaptive nonlinear diffusion in wavelet domain”, J. Electronic Imaging, **20**, 14 (2011).
[12] A.C.-C Shih, H.-Y.M., Liao, C.-S. Lu, ”A New Iterated Two-Band Diffusion Equation: Theory and Its Applications”, IEEE Transactions on Image Processing, **4**, 466-476 (2003).
[13] M. Aharon, M. Elad and A. M. Bruckstein, ”The K-SVD: An Algorithm for Designing of Overcomplete Dictionaries for Sparse Representation”, IEEE Transactions on Signal Processing, **54**, 4311-4322 (2006).
[14] P. Chatterjee and P. Milanfar, Clustering-based Denoising with Locally Learned Dictionaries (K-LLD), IEEE Transactions on Image Processing, **18**, 1438-1451 (2009).
[15] K. Dabov, A. Foi, V. Katkovnik, and K. Egiazarian, ”Image denoising by sparse 3D transform-domain collaborative filtering”, IEEE Transactions on Image Processing, **16**, 2080-2095 (2007).
[16] J. Mairal, F. Bach, J. Ponce, G. Sapiro, and A. Zisserman, ”Non-Local Sparse Models for Image Restoration,” Proceedings of ICCV, (2009).
[17] G. Gilboa, S. Osher, ”Nonlocal operators with applications to image processing”, Multiscale Modeling and Simulation, **7**, 1005-1028 (2009).
[18] G. Peyre, ”Image Processing with Non-Local Spectral Bases”, SIAM Journal on Multiscale Modeling and Simulation, **7**, 703-730 (2008).
[19] X. Zhang, M. Burger, X. Bresson, and S. Osher, ”Bregmanized Nonlocal Regularization for Deconvolution and Sparse Reconstruction”, SIAM Journal on Imaging Sciencesvol, **3**, 253-276 (2010).
[20] K. Dabov, A. Foi, V. Katkovnik, and K. Egiazarian, ”A nonlocal and shape-adaptive transform-domain collaborative filtering”, In Proc. Int. Workshop on Local and Non-Local Approx. in Image Process., LNLA (2008).
[21] C.-A. Deledalle, V. Duval and J. Salmon, ”Non-Local Methods with Shape-Adaptive Patches (NLM-SAP)”, Journal of Mathematical Imaging and Vision, 1-18 (2011).
[22] R. Achanta, A. Shaji, K. Smith, A. Lucchi, P. Fua, S. Susstrunk, ”SLIC Superpixels Compared to State-of-the-Art Superpixel Methods”, IEEE Transactions on Pattern Analysis and Machine Intelligence, **34**, 2274-2282 (2012).
[23] G.R.J. Cooper, ”The Antialiased Textural Analysis of Aeromagnetic Data”, Computers and Geosciences, **35**, 586-591 (2009).
[24] B. Levin and B. Nadler, ”Natural Image Denoising: Optimality and Inherent Bounds”, In IEEE Conference on Computer Vision and Pattern Recognition (CVPR 2011), (2011).
[25] P. Chatterjee and P. Milanfar, ”Is Denoising Dead?”, IEEE Transactions on Image Processing, **19**, 895-911 (2010).
[26] J. Immerkaer, ”Fast Noise Variance Estimation, Computer Vision and Image Understanding”, **4**, 300-302 (1996).
[27] G. Gilboa, N. Sochen, and Y. Y. Zeevi, ”Forward-and-backward diffusion processes for adaptive image enhancement and denoising”, IEEE Transactions om Image Processing, **11**, 689-703 (2002).
[28] Y. Wang , R. Niu , L. Zhang and H. Shen , ”Region-based adaptive anisotropic diffusion for image enhancement and denoising’, Opt. Eng., **49**, 11 (2010).
[29] Z. Wang and AC Bovik, ”A universal image quality index,” IEEE Signal Processing Letters, (2002).

Ajay K. Mandava received his MS degree in electrical engineering from University of Nevada, Las Vegas, Nevada, in 2009. Currently, he is working toward his PhD in the Department of Electrical and Computer Engineering, University of Nevada, Las Vegas, Nevada. His work focuses on adaptive image enhancement and restoration, and efficient design and realization of image processing algorithms.

Emma E. Regentova has obtained her PhD in computer engineering from State Engineering University of Armenia. Currently, she is an associate professor in the Electrical and Computer Engineering Department, University of Nevada, Las Vegas, Nevada. She is active in applied image processing, data compression, and advanced computer architectures.

George Bebis has obtained his B.S. degree in mathematics and the M.S. degree in computer science from the University of Crete, Greece, in 1987 and 1991, respectively, and the Ph.D. degree in electrical and computer engineering from the University of Central Florida, Orlando, in 1996. Currently, he is a Professor in the Department of Computer Science and Engineering at the University of Nevada, Reno (UNR), Director of the UNR Computer Vision Laboratory (CVL), and Visiting Professor at King Saud University. Prior to joining UNR, he was a Visiting Assistant Professor in the Department of Mathematics and Computer Science at the University of Missouri-St. Louis (UMSL).His research interests include computer vision, image processing, pattern recognition, machine learning, and evolutionary computing. His research has been funded by NSF, NASA, ONR, NIJ, and Ford Motor Company. Dr. Bebis is an Associate Editor of the Machine Vision and Applications journal and serves on the editorial boards of the International Journal on Artificial Intelligence Tools and the Computer Methods in Biomechanics and Biomedical Engineering: Imaging and Visualization journal. He has served on the program committees of various national and international conferences and has organized and chaired several conference sessions. In 2002, he received the Lemelson Award for Innovation and Entrepreneurship.